Effective Polyakov Loop Dynamics for Finite Temperature G_2 Gluodynamics

Björn H. Wellegehausen, Andreas Wipf, and Christian Wozar*

Theoretisch-Physikalisches Institut, Friedrich-Schiller-Universität Jena, Max-Wien-Platz 1, 07743 Jena, Germany

Based on the strong coupling expansion we obtain effective 3-dimensional models for the Polyakov loop in finite temperature G_2 gluodynamics. The Svetitsky-Jaffe conjecture relates the resulting continuous spin models with G_2 gluodynamics near phase transition points. In the present work we analyse the effective theory in leading order with the help of a generalised mean field approximation and with detailed Monte Carlo simulations. In addition we derive a Potts-type discrete spin model by restricting the characters of the Polyakov loops to the three extremal points of the fundamental domain of G_2. Both the continuous and discrete effective models show a rich phase structure with a ferromagnetic, symmetric and several anti-ferromagnetic phases. The phase diagram contains first and second order transition lines and tricritical points. The modified mean field predictions compare very well with the results of our simulations.

I. INTRODUCTION

For many good reasons G_2 gluodynamics has attracted much attention recently. For example, the 14-dimensional exceptional group G_2 has a trivial centre, in contrast to the usually studied $SU(N)$ gauge groups. Indeed it is the smallest simple and simply connected compact Lie group with this property. Thus G_2 gluodynamics is useful to better understand the relevance of the centre symmetry for confinement [1]. Actually a non-trivial centre is needed in several proposed scenarios for confinement and hence G_2 gluodynamics can be used to test these proposals. It has been convincingly demonstrated that the theory shows a first order finite temperature transition without order parameter from a confining to a deconfining phase which can be explained by centre vortices [2]. In this context confinement refers to confinement at intermediate scales, where a Casimir scaling of string tensions has been reported [3]. But on large scales, deep in the infrared, strings break due to gluon production and the static inter-quark potential becomes flat [4]. Recently it has been demonstrated that chiral symmetry is broken at low temperatures and is restored at high temperatures at the thermodynamic phase transition [5].

G_2 gluodynamics has an intriguing connection to $SU(3)$ gauge theory. When one couples a scalar field in the 7-dimensional fundamental representation to the gauge field one can break the G_2 gauge symmetry to the $SU(3)$ gauge symmetry of strong interaction. With increasing hopping parameter κ the resulting Yang-Mills-Higgs theory interpolates smoothly between G_2 gluodynamics without centre symmetry and $SU(3)$ gluodynamics with $\mathbb{Z}_3$ centre symmetry. For intermediate values of the hopping parameter the theory mimics $SU(3)$ gauge theory with dynamical quarks and the masses of these 'quarks' increase with increasing hopping parameter. In G_2 gluodynamics the Polyakov loop is no longer an order parameter in the strict sense. Despite this fact it still serves as

*Electronic addresses:
Bjoern.Wellegehausen@uni-jena.de, wipf@tpi.uni-jena.de and
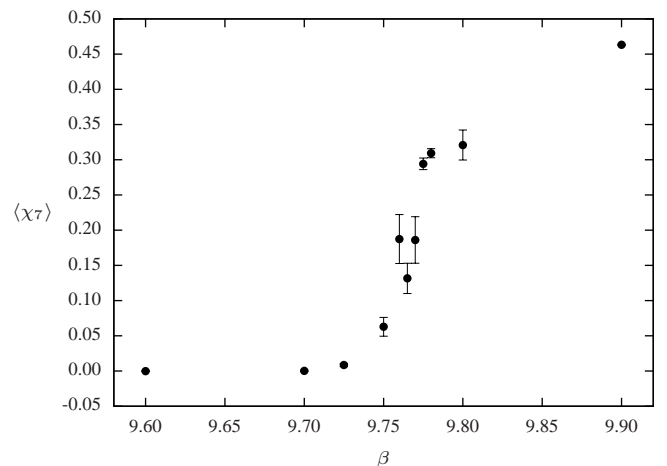Christian.Wozar@uni-jena.de

FIG. 1: Expectation value of the traced Polyakov loop in the fundamental 7-dimensional representation in G_2 gluodynamics on a $16^3 \times 6$ lattice as obtained via hybrid Monte Carlo sampling. The phase transition is located for the Wilson action at a critical $\beta_c \approx 9.765$.

an approximate order parameter separating the confined from the deconfined phase (see Fig. 1) with a rapid change at the phase transition point.

According to the conjecture by Svetitsky and Yaffe [6, 7] the dynamics at the finite temperature confinement-deconfinement transition of a $d+1$-dimensional pure gauge theory can be described by an effective spin model in d dimensions. Based on our earlier results on finite temperature $SU(2)$ and $SU(3)$ gluodynamics [8–12] there are strong indications that the effective models derived and analysed in the present work are sufficient to accurately describe the dynamics of Polyakov loops. The direct connection between the effective spin models and G_2 gluodynamics is postponed to a forthcoming publication.

In Sec. II we review kinematic aspects of G_2 and the main implications for G_2 gluodynamics. Afterwards in Sec. III the strong coupling expansion for the effective Polyakov loop action is explained and in particular the effective theory in leading order is introduced. In Sec. IV we investigate the properties of the effective model first by a classical analysis, then by

a modified mean field approximation and finally by extensive Monte Carlo simulations. Reducing the continuous spin degrees further to the discrete spins situated at the 3 edges of the fundamental domain of G_2 we end up with a deformed Potts-type spin model whose phase diagram is explored in Sec. V.

II. THE GROUP G_2

G_2 is the smallest of the five exceptional simple Lie groups and can be viewed as a subgroup of $SO(7)$ subject to seven independent cubic constraints for the 7-dimensional matrices g representing $SO(7)$ [13]:

$$T_{abc} = T_{def}\, g_{da}\, g_{eb}\, g_{fc}. \tag{1}$$

Here T is a total antisymmetric tensor given by

$$T_{127} = T_{154} = T_{163} = T_{235} = T_{264} = T_{374} = T_{576} = 1. \tag{2}$$

The constraints (1) for the group elements reduce the 21 generators of $SO(7)$ to 14 generators of the group G_2 with rank 2. Its fundamental representations are the defining 7-dimensional and the adjoint 14-dimensional representation with Dynkin labels

$$(7) = [1,0], \quad (14) = [0,1]. \tag{3}$$

G_2 has a trivial centre and its Weyl group is the dihedral group D_6 of order 12. Additionally G_2 is connected to $SU(3)$ through the embedding of $SU(3)$ as a subgroup of G_2 according to [14]

$$G_2/SU(3) \sim SO(7)/SO(6) \sim S_6. \tag{4}$$

So when the S_6 part of G_2 is frozen out[1] we end up at $SU(3)$ gauge theory.

In effective theories for the gauge invariant (traced) Polyakov loops in the fundamental representations we are aiming at, only the reduced Haar measure is needed. Based on [15] this measure can be given for a parametrisation of the conjugacy classes either by angular variables or alternatively by the fundamental characters,

$$d\mu \propto J^2 d\varphi_1\, d\varphi_2 = J\, d\chi_7\, d\chi_{14}. \tag{5}$$

The density J^2 can be expressed in terms of the fundamental characters,

$$J^2 = \left(4\chi_7^3 - \chi_7^2 - 2\chi_7 - 10\chi_7\chi_{14} + 7 - 10\chi_{14} - \chi_{14}^2\right) \\ \times \left(7 - \chi_7^2 - 2\chi_7 + 4\chi_{14}\right), \tag{6}$$

---

[1] This is possible when a fundamental Higgs field is coupled to the gauge field [1].

where the characters are given in terms of (particularly chosen) angular variables $\varphi_{1,2}$ as

$$\chi_7 = 1 + 2\cos(\varphi_1) + 2\cos(\varphi_2) + 2\cos(\varphi_1 + \varphi_2),$$
$$\chi_{14} = 2\big(1 + \cos(\varphi_1) + \cos(\varphi_1 - \varphi_2) + \cos(\varphi_2) \\ + \cos(\varphi_1 + \varphi_2) + \cos(2\varphi_1 + \varphi_2) + \cos(\varphi_1 + 2\varphi_2)\big). \tag{7}$$

The boundary of the fundamental domain is determined by $J = 0$ and thus is parametrised by the three curves (see Fig. 2)

$$\chi_{14} = \frac{1}{4}(\chi_7 + 1)^2 - 2,$$
$$\chi_{14} = -5(\chi_7 + 1) \pm 2(\chi_7 + 2)^{3/2}. \tag{8}$$

Note that the reduced G_2 Haar measure is maximal not at the origin but for $(\chi_7, \chi_{14}) = (-1/5, -2/5)$. The fundamental domain has no symmetries at all and this expresses the fact that the centre of G_2 is trivial.

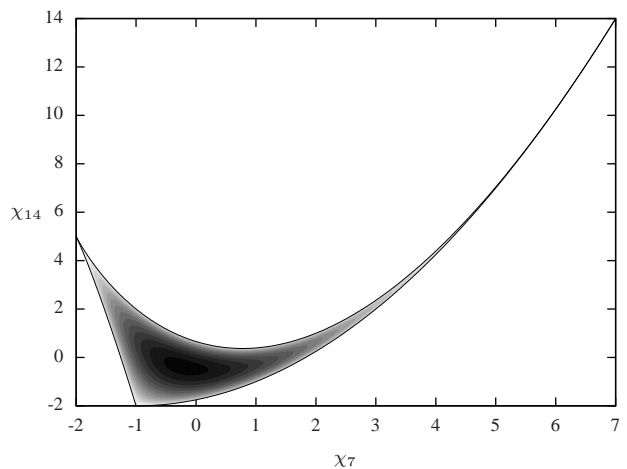

FIG. 2: Fundamental domain of G_2. Darker regions indicate a bigger Haar measure.

Representation theory and implications for confinement

In the pioneering work [13] the confining properties of G_2 have been discussed and compared to those of $SU(3)$. Quarks and anti-quarks in $SU(3)$ transform under the fundamental representations 3 and $\bar{3}$ such that their charges can only be screened by particles with non-vanishing 3-ality, especially *not by gluons*. This explains why in the confining phase of $SU(3)$ gluodynamics the static inter-quark potential is linearly rising up to arbitrary long distances. As a consequence the free energy of a single quark gets infinite and the Polyakov loop expectation value vanishes. Hence the Polyakov loop discriminates the confining from the deconfining phase and at the same time serves as order parameter for the $\mathbb{Z}_3$ centre symmetry.

To better understand G_2 gluodynamics we recall the decomposition of tensor products into irreducible representa-

tions,

$$(7) \otimes (7) = (1) \oplus (7) \oplus (14) \oplus (27)$$
$$(7) \otimes (7) \otimes (7) = (1) \oplus 4 \cdot (7) \oplus 2 \cdot (14) \oplus 3 \cdot (27)$$
$$\oplus \, 2 \cdot (64) \oplus (77)$$
$$(14) \otimes (14) = (1) \oplus (14) \oplus (27) \oplus (77) \oplus (77')$$
$$(14) \otimes (14) \otimes (14) = (1) \oplus (7) \oplus 5 \cdot (14) \oplus 3 \cdot (27) \oplus \cdots$$
$$(9)$$

with Dynkin labels

$$(1) = [0,0], \quad (27) = [2,0], \quad (64) = [1,1],$$
$$(77) = [3,0], \quad (77') = [0,2]. \tag{10}$$

The quarks in G_2 transform under the 7-dimensional fundamental representation, gluons under the 14-dimensional fundamental (and at the same time adjoint) representation. From (9) we see that similarly as in $SU(3)$ two or three quarks can build a colour singlet (meson or baryon, respectively). In G_2 gluodynamics three centre-blind dynamical gluons can screen the colour charge of a single quark,

$$(7) \otimes (14) \otimes (14) \otimes (14) = (1) \oplus \cdots . \tag{11}$$

Thus the flux tube between two static quarks can break due to gluon production and the Polyakov loop does not vanish even in the confining phase [1]. This shows that the Polyakov loop can at best be an approximate order parameter (see Fig. 1) which changes rapidly at the phase transition and is small (but non-zero) in the confining phase. To characterise confinement we can no longer refer to a non-vanishing asymptotic string tension and vanishing Polyakov loop. Instead we define confinement as the absence of free colour charges in the physical spectrum. In the confining phase the inter-quark potential rises linearly at intermediate scales [2, 3].

III. EFFECTIVE THEORIES AND THE STRONG COUPLING EXPANSION

Based on a conjecture relating finite temperature $SU(N)$ gluodynamics in $d+1$ dimensions at the critical point with a $\mathbb{Z}_N$ spin model in d dimensions [6, 7], there have been extended studies to compare correlation functions of both systems for $SU(2)$ [9–11] and $SU(3)$ gluodynamics [8, 12], either by using Schwinger-Dyson equations or demon methods [16, 17]. The strong coupling expansion for the distribution of the inhomogeneous Polyakov loops was taken as ansatz for the (exponentiated) effective Polyakov-loop action. This way effective models for $SU(3)$ gluodynamics have been derived in [8]. Here we sketch how one arrives at the analogous results for G_2 and obtain the effective continuous spin model in leading order.

Starting with the lattice Wilson action

$$S_{\mathrm{W}} = \beta \sum_{\square} \left(1 - \frac{1}{N_{\mathrm{C}}} \operatorname{Re} \operatorname{tr} U_{\square} \right), \quad \beta = \frac{2N_{\mathrm{C}}}{a^4 g^2}, \quad N_{\mathrm{C}} = 7 \tag{12}$$

a *strong coupling expansion* (for small β) is performed to arrive at an effective theory for the local Polyakov loops. To

do that one inserts a group valued delta function into the path integral,

$$Z = \int \mathcal{D}U \exp(-S_{\mathrm{W}}[U])$$
$$= \int \mathcal{D}P \int \mathcal{D}U \, \delta \left(P_{\boldsymbol{x}}, \prod_{\tau=1}^{N_{\mathrm{t}}} U_{\tau,\boldsymbol{x}} \right) \exp(-S_{\mathrm{W}}[U]) \tag{13}$$
$$\equiv \int \mathcal{D}P \, \exp(-S_{\mathrm{eff}}[\mathcal{P}]).$$

Here $\mathcal{D}P$ denotes the product of reduced Haar measures on the sites of the *spatial lattice*. We do not need the full Haar measure of G_2 since the effective action S_{eff} only depends on the gauge invariant content of the local Polyakov loop.

In compact form the strong coupling expansion is then given by

$$S_{\mathrm{eff}}[\mathcal{P}] = \sum_r \sum_{\mathcal{R}_1 \ldots \mathcal{R}_r} \sum_{\ell_1 \ldots \ell_r} c_{\mathcal{R}_1 \ldots \mathcal{R}_r}^{\ell_1 \ldots \ell_r}(\beta) \prod_{i=1}^r S_{\mathcal{R}_i, \ell_i}$$
$$= \sum_i \lambda_i S_i \tag{14}$$

with the basic building blocks

$$S_{\mathcal{R}, \ell} \equiv \chi_{\mathcal{R}}(\mathcal{P}_{\boldsymbol{x}}) \chi_{\mathcal{R}}^*(\mathcal{P}_{\boldsymbol{y}}) + \text{c.c.}, \quad \ell \equiv \langle \boldsymbol{x} \boldsymbol{y} \rangle. \tag{15}$$

Here r counts the number of link operators contributing at each order. The coefficients $c_{\mathcal{R}_1 \ldots \mathcal{R}_r}^{\ell_1 \ldots \ell_r}$ couple the operators $S_{\mathcal{R}_i, \ell_i}$ sitting at nearest neighbour links $\ell_i \equiv \langle \boldsymbol{x}_i, \boldsymbol{y}_i \rangle$ in representation $\mathcal{R}_i$. The effective action hence describes a *network of link operators* that are collected into (possibly disconnected) 'polymers' contributing with 'weight' $c_{\mathcal{R}_1 \ldots \mathcal{R}_r}^{\ell_1 \ldots \ell_r}$. The resulting 'operators' (Polyakov loop monomials) are *dimensionless* and there is *no natural* ordering scheme at hand. Our chosen truncation is based on the strong coupling expansion in powers of β which is closely related to the dimension of the corresponding group representations and the distance across which the Polyakov loops are coupled. In the strong coupling expansion truncated at $\mathcal{O}(\beta^{kN_{\mathrm{t}}})$ one has $r \leq k$ and the additional restriction $|\mathcal{R}_1| + \cdots + |\mathcal{R}_r| < k$ with $|\mathcal{R}| \equiv p_1 + p_2$ for a given representation $\mathcal{R}$ of G_2 with Dynkin labels $[p_1, p_2]$. The leading order terms only contain interactions between nearest neighbours $\langle \boldsymbol{x} \boldsymbol{y} \rangle$ and the two fundamental representations.

For $SU(3)$ the characters of the two fundamental representations are complex conjugate of each other such that the effective Polyakov loop action contains just one term in leading order. In G_2 this situation changes and we find two independent contributions in leading order. We refer to the corresponding model containing the two fundamental representations as *fundamental model*. Its action is explicitly given by

$$S_{\mathrm{eff}} = \lambda_7 \underbrace{\sum_{\langle \boldsymbol{x} \boldsymbol{y} \rangle} \chi_7(\mathcal{P}_{\boldsymbol{x}}) \chi_7(\mathcal{P}_{\boldsymbol{y}})}_{S_7} + \lambda_{14} \underbrace{\sum_{\langle \boldsymbol{x} \boldsymbol{y} \rangle} \chi_{14}(\mathcal{P}_{\boldsymbol{x}}) \chi_{14}(\mathcal{P}_{\boldsymbol{y}})}_{S_{14}}, \tag{16}$$

where the couplings λ_7 and λ_{14} are indexed by the dimension of the involved representation. In next-to leading order there

exist six additional terms with nearest neighbour interactions. Their explicit forms are dictated by representation theory (9)

$$S_{27} = \sum_{\langle \boldsymbol{xy} \rangle} \chi_{27}(\mathcal{P}_{\boldsymbol{x}}) \chi_{27}(\mathcal{P}_{\boldsymbol{y}}),$$

$$S_{77'} = \sum_{\langle \boldsymbol{xy} \rangle} \chi_{77'}(\mathcal{P}_{\boldsymbol{x}}) \chi_{77'}(\mathcal{P}_{\boldsymbol{y}}),$$

$$S_{64} = \sum_{\langle \boldsymbol{xy} \rangle} \chi_{64}(\mathcal{P}_{\boldsymbol{x}}) \chi_{64}(\mathcal{P}_{\boldsymbol{y}}),$$

$$S_{7,7} = \sum_{\langle \boldsymbol{xy} \rangle} \left(\chi_7(\mathcal{P}_{\boldsymbol{x}}) \chi_7(\mathcal{P}_{\boldsymbol{y}}) \right)^2, \quad (17)$$

$$S_{14,14} = \sum_{\langle \boldsymbol{xy} \rangle} \left(\chi_{14}(\mathcal{P}_{\boldsymbol{x}}) \chi_{14}(\mathcal{P}_{\boldsymbol{y}}) \right)^2,$$

$$S_{7,14} = \sum_{\langle \boldsymbol{xy} \rangle} \chi_7(\mathcal{P}_{\boldsymbol{x}}) \chi_7(\mathcal{P}_{\boldsymbol{y}}) \chi_{14}(\mathcal{P}_{\boldsymbol{x}}) \chi_{14}(\mathcal{P}_{\boldsymbol{y}}).$$

It the remainder of this work we shall neglect the next-lo leading order terms and concentrate on the fundamental model (16).

IV. THE FUNDAMENTAL MODEL

For the fundamental effective model (16) we shall localise the symmetric, ferromagnetic and anti-ferromagnetic phases with coexistence lines in order to find the region in the space of couplings λ_7, λ_{14} where a connection to G_2 gluodynamics can be established.

A. Classical analysis

For strong couplings the fluctuations of the Polyakov loops are suppressed and the spin system behaves almost classically. Thus for large $|\lambda_7|$ and $|\lambda_{14}|$ we may compute the phase diagram by minimising the classical action. Anticipating that there are anti-ferromagnetic phases we introduce the odd and even sublattices

$$\Lambda_o = \{ \boldsymbol{x} \,|\, x_1 + x_2 + x_3 \text{ odd} \} \quad \text{and}$$
$$\Lambda_e = \{ \boldsymbol{x} \,|\, x_1 + x_2 + x_3 \text{ even} \}. \quad (18)$$

On each sublattice the Polyakov loop is assumed to have a *constant* value and the two values are denoted by $\mathcal{P}_o$ and $\mathcal{P}_e$, respectively. We denote the corresponding characters in the fundamental domain of G_2 by

$$\boldsymbol{\chi}_e = \begin{pmatrix} \chi_{7,e} \\ \chi_{14,e} \end{pmatrix} = \begin{pmatrix} \chi_7 \\ \chi_{14} \end{pmatrix} (\mathcal{P}_e) \quad \text{and}$$

$$\boldsymbol{\chi}_o = \begin{pmatrix} \chi_{7,o} \\ \chi_{14,o} \end{pmatrix} = \begin{pmatrix} \chi_7 \\ \chi_{14} \end{pmatrix} (\mathcal{P}_o). \quad (19)$$

With this assumption and notation the action of the fundamental model (16) reads

$$S_{\text{eff}} = V \boldsymbol{\chi}_e^{\mathsf{T}} K \boldsymbol{\chi}_o \quad \text{with} \quad K = 3 \begin{pmatrix} \lambda_7 & 0 \\ 0 & \lambda_{14} \end{pmatrix}. \quad (20)$$

To localise the different phases we may assume that the Polyakov loop on one sublattice, say Λ_o, is equal to the group-identity with maximal characters, $\chi_{7,o} = 7$ and $\chi_{14,o} = 14$. For given couplings λ_7 and λ_{14} the corresponding thermodynamic phase is then determined by that Polyakov loop on Λ_e for which the linear function $7\lambda_7 \chi_{7,e} + 14\lambda_{14} \chi_{14,e}$ is minimal. If the minimising characters are the same on both sublattices then the phase is ferromagnetic, else it is anti-ferromagnetic. The minimum of the linear function is attained for χ_e on one of the three corners of the fundamental domain in Fig. 2 or on the curve connecting the corners $(-1, -2)^{\mathsf{T}}$ and $(7, 14)^{\mathsf{T}}$. Depending on the sign of λ_7 and the slope $\xi \equiv \lambda_{14}/\lambda_7$ one finds the following phases:

- For $\lambda_7 > 0$ and $\xi < -1/2$ or for $\lambda_7 < 0$ and $\xi > -1/8$ we find the *ferromagnetic phase* F with $\chi_e^{\mathsf{T}} = (7, 14)$.

- For $\lambda_7 > 0$ and $\xi > 1/14$ we find a *anti-ferromagnetic phase* AF1 with $\chi_e^{\mathsf{T}} = (-1, -2)$.

- For $\lambda_7 > 0$ and $-1/2 < \xi < 1/14$ we find a second *anti-ferromagnetic phase* AF2 with $\chi_e^{\mathsf{T}} = (-2, 5)$.

- For $\lambda_7 < 0$ and $\xi < -1/8$ the characters $\chi_e^{\mathsf{T}} = (-1 - 1/\xi, 1/(2\xi)^2 - 2)$ change continuously from $(7, 14)$ to $(-1, -2)$ along the connecting boundary curve of the fundamental domain. This *transition phase* is denoted by F $\rightarrow$ AF1.

The phase portrait is depicted in Fig. 3 where we also included the expected symmetric phase for weak couplings. Since in a symmetric phase entropy wins over energy it cannot be seen in any classical analysis.
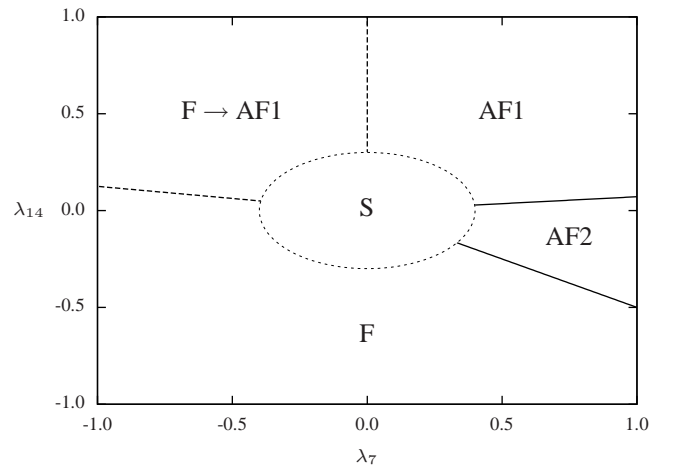

FIG. 3: The classical phase diagram of the fundamental effective G_2 model. In addition to the calculated ferromagnetic and anti-ferromagnetic phases we expect a symmetric phase for weak couplings.

B. Mean field analysis

The classical analysis is refined by a modified mean field approximation in which one allows for inhomogeneous mean

fields. First we recall the main aspects of the method. Here we are interested in expectation values of the form

$$\langle A \rangle = \frac{1}{Z} \int \mathcal{DP} \exp(-S_{\text{eff}}[\mathcal{P}]) A[\mathcal{P}],$$
$$\mathcal{DP} \equiv \prod_{\boldsymbol{x}} d\mu(\mathcal{P}_{\boldsymbol{x}}), \tag{21}$$

where the gauge invariant function $A(\mathcal{P})$ depends on the Polyakov loop via the the fundamental characters $\chi_7(\mathcal{P})$ and $\chi_{14}(\mathcal{P})$ and $d\mu$ is the reduced Haar measure of G_2. The equilibrium probability measure $\mathcal{DP} \exp(-S_{\text{eff}})/Z$ is the unique minimum to the variational problem

$$\inf_p \langle S_{\text{eff}} + \ln p \rangle_p, \tag{22}$$

where the p-indexed expectation value is calculated with the integration measure $p[\mathcal{P}] \mathcal{DP}$, whose probability density p is to be varied. Expectation values of observables can then be computed as

$$\langle A \rangle_p = \int \mathcal{DP} \, p[\mathcal{P}] A[\mathcal{P}]. \tag{23}$$

In this scope a Monte Carlo simulation is just the approximation of the probability density $p[\mathcal{P}] \propto \exp(-S_{\text{eff}}[\mathcal{P}])$ with a finite set of configurations which give $p[\mathcal{P}] \approx N_{\text{MC}}^{-1} \times \sum_{t=1}^{N_{\text{MC}}} \delta(\mathcal{P} - \mathcal{P}_t)$, where $\mathcal{P}_t$ is the configuration in the t'th Monte Carlo step and N_{MC} is the number of Monte Carlo steps.

In a variational approach the mean field approximation amounts to the restriction of the admissible densities p to product form

$$p[\mathcal{P}] \to \prod_{\boldsymbol{x}} p_{\boldsymbol{x}}(\mathcal{P}_{\boldsymbol{x}}). \tag{24}$$

Then expectation values factorise and the computation can be done site by site. Due to the translational invariance of the action one may believe, that the minimising density is translational invariant, $p_{\boldsymbol{x}}(\mathcal{P}) = p(\mathcal{P})$. However, this assumption is only justified for the symmetric and ferromagnetic phases with constant mean fields.

Anticipating the existence of additional anti-ferromagnetic phases we partition the lattice into its even and odd sublattices, as we did in the classical analysis, and allow for different densities on the sublattices,

$$p_{\boldsymbol{x}}(\mathcal{P}_{\boldsymbol{x}}) = \begin{cases} p_{\text{e}}(\mathcal{P}_{\boldsymbol{x}}) & : \boldsymbol{x} \in \Lambda_{\text{e}} \\ p_{\text{o}}(\mathcal{P}_{\boldsymbol{x}}) & : \boldsymbol{x} \in \Lambda_{\text{o}} \end{cases}. \tag{25}$$

The classical analysis is then recovered by allowing only δ-type point-measures for $p_{\text{e,o}}$. In the modified mean-field analysis we allow for all $p_{\text{e,o}}$ in the variational principle with prescribed mean fields $\bar{\boldsymbol{\chi}}_{\text{e}}$ and $\bar{\boldsymbol{\chi}}_{\text{o}}$ on the even and odd sublattices. The effective potential u is then obtained by computing

$$u(\bar{\boldsymbol{\chi}}_{\text{e}}, \bar{\boldsymbol{\chi}}_{\text{o}}) = \frac{1}{V} \inf_p \langle S_{\text{eff}} + \ln p \rangle_p, \tag{26}$$

subject to the following four constraints for the admitted densities p_{e} and p_{o}:

$$\langle \boldsymbol{\chi} \rangle_{\text{e,o}} = \bar{\boldsymbol{\chi}}_{\text{e,o}}. \tag{27}$$

The one-site expectation values $\langle \ldots \rangle_{\text{e,o}}$ are calculated with $p_{\text{e,o}} \, d\mu$. To actually compute the minimising densities one needs the expectation value of the action and entropy, given by

$$\langle S_{\text{eff}} \rangle_p = V \bar{\boldsymbol{\chi}}_{\text{e}}^{\mathsf{T}} K \bar{\boldsymbol{\chi}}_{\text{o}},$$
$$\langle \ln p \rangle_p = \frac{V}{2} \langle \ln p_{\text{e}} \rangle_{\text{e}} + \frac{V}{2} \langle \ln p_{\text{o}} \rangle_{\text{o}}, \tag{28}$$

where K is the matrix given in (20). On each sublattice the variational problem is solved by a density $p \propto \exp(\boldsymbol{j} \cdot \boldsymbol{\chi}(\mathcal{P}))$ with two Lagrangian multipliers $\boldsymbol{j} = (j_7, j_{14})$. The four multipliers are determined by the four constraints in (27). Using this solution for the densities in the variational principle determines the effective potential as function of the prescribed mean fields. The expectation values of the characters on the two sublattices minimise the effective potential. These minimas solve the following system of coupled gap equations

$$K \bar{\boldsymbol{\chi}}_{\text{e}} = -\frac{\partial w(\bar{\boldsymbol{\chi}}_{\text{o}})}{\partial \bar{\boldsymbol{\chi}}_{\text{o}}}, \quad K \bar{\boldsymbol{\chi}}_{\text{o}} = -\frac{\partial w(\bar{\boldsymbol{\chi}}_{\text{e}})}{\partial \bar{\boldsymbol{\chi}}_{\text{e}}},$$
$$w(\bar{\boldsymbol{\chi}}) = \ln \int d\mu(\mathcal{P}) \, e^{-\bar{\boldsymbol{\chi}}^{\mathsf{T}} K \boldsymbol{\chi}(\mathcal{P})}. \tag{29}$$

We have calculated the expectation values of χ_7 and χ_{14} on both sublattices as functions of the couplings on a 120×100 grid in the rectangle

$$-0.3 \leq \lambda_7 \leq 0.3 \quad \text{and} \quad -0.25 \leq \lambda_{14} \leq 0.25. \tag{30}$$

The contour plot of the expectation value

$$\langle \chi_7 \rangle = \frac{1}{2} \left(\langle \chi_{7,\text{e}} \rangle + \langle \chi_{7,\text{o}} \rangle \right), \tag{31}$$

called *magnetisation*, is depicted in Fig. 4. As expected, for weak couplings we find a symmetric phase with vanishing magnetisation in the centre of the phase diagram. On the lower left, for negative couplings, we find the ferromagnetic phase with $\langle \chi_{7,\text{e}} \rangle = \langle \chi_{7,\text{o}} \rangle \approx 7$ or equivalently with a typical $\mathcal{P}_{\boldsymbol{x}}$ near the identity. For an unambiguous identification of the phases one needs the expectation values of both χ_7 and χ_{14} on both sublattices. We have calculated these four expectation values for the fundamental model on a grid in the space of coupling constants with extensive Monte Carlo simulations. Since the numerical simulations and mean field approximation yield almost identical results we defer the detailed discussion of phase portrait, and in particular the localisation of the various anti-ferromagnetic phases for positive couplings, to the following section.

C. Monte Carlo results

We performed our Monte Carlo simulations with about $10\,000$ samples for every point on a 60×50 grid inside the rectangle
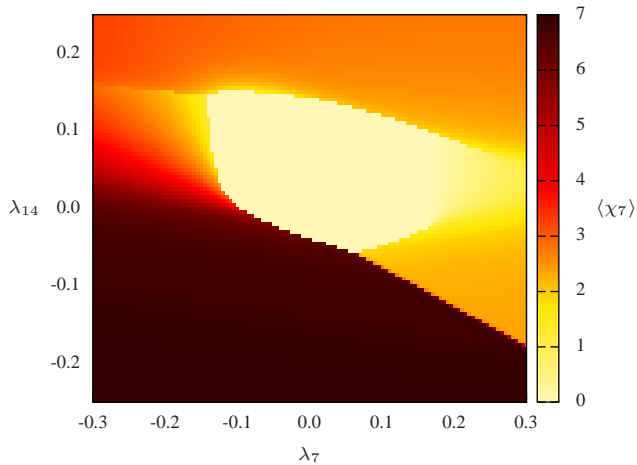
FIG. 4: (Colour online) Polyakov loop $\langle\chi_7\rangle$ of the *fundamental G_2* spin model in mean field approximation.

(30) in the space of coupling constants. Two neighbouring points on this grid are separated by 0.01. First we calculated the magnetisation $\langle\chi_7\rangle$ and the resulting phase portrait is depicted in Fig. 5. It looks very similar to the portrait calculated in the mean field approximation, see Fig. 4. For weak
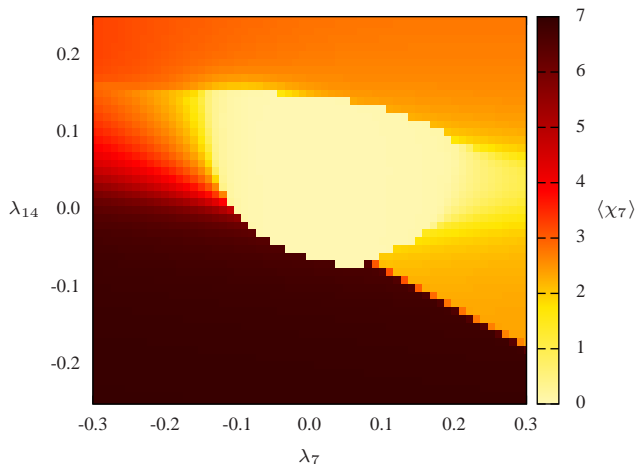

FIG. 5: (Colour online) Polyakov loop $\langle\chi_7\rangle$ of the fundamental model obtained via Monte Carlo simulation on an 8^3 lattice.

couplings entropy wins over energy and the product of Haar measures of the Polyakov loops become relevant. In order to unambiguously identify the anti-ferromagnetic phases for positive couplings we again subdivided the lattice in the even and odd sublattice, $\Lambda = \Lambda_e \cup \Lambda_o$, and measured the *staggered magnetisation*

$$S = \frac{1}{2}\langle|\chi_{7,e} - \chi_{7,o}|\rangle. \tag{32}$$

The corresponding contour plot is exhibited in Fig. 6. On top and on the right of the plot the staggered magnetisation gets large and we identify this region as belonging to anti-ferromagnetic phases. For large absolute values of λ_7, λ_{14} action (energy) dominates over entropy and this explains why
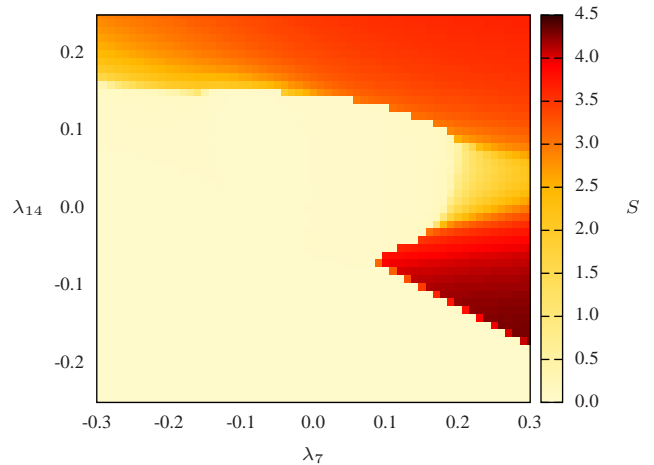
the simulation results agree well with the classical analysis for strong couplings: all phases but the *transition phase* F → AF1 are already visible in the classical phase diagram in Fig. 3. In the Monte Carlo simulation an additional "symmetric phase" with vanishing Polyakov loop and vanishing staggered magnetisation appears for weak couplings, in complete agreement with our mean field analysis. The resulting phase diagram with one symmetric, one ferromagnetic and two anti-ferromagnetic phases is depicted in Fig. 7.

FIG. 6: (Colour online) Staggered magnetisation S of the fundamental model obtained via Monte Carlo simulation on an 8^3 lattice.
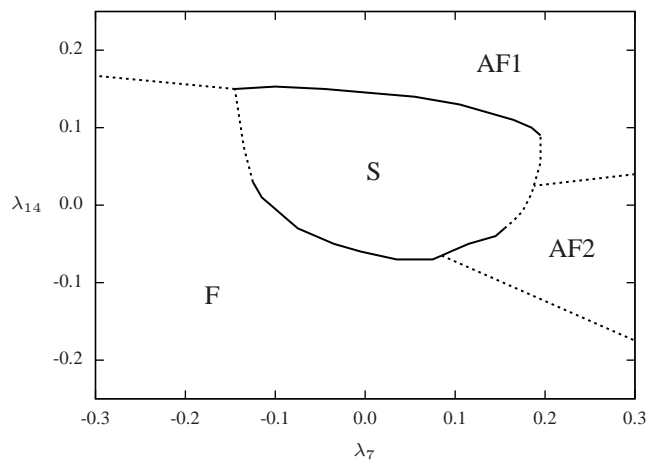

FIG. 7: Phase diagram of the fundamental effective model. The orders of phase transitions are indicated with full lines (first order) and dotted lines (second order/crossover).

Eventually the finite temperature phase transition in G_2 gluodynamics will correspond to a transition between the symmetric and the ferromagnetic phase in the effective spin model. The dependence of the effective couplings λ_7, λ_{14} on the Yang-Mills coupling β can be calculated with the help of powerful inverse Monte Carlo techniques [8, 12]. This will be done in a forthcoming publication. However, we anticipate that the confinement-deconfinement phase transition in G_2 gluodynamics will happen near the critical point
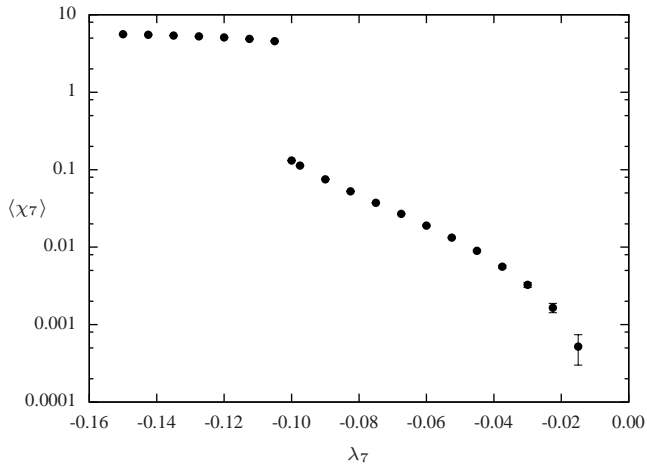
FIG. 8: Polyakov loop $\langle\chi_7\rangle$ of the fundamental effective model with coupling $\lambda_{14} = 0$ obtained via Monte Carlo simulation on an 8^3 lattice.

FIG. 9: Distribution of χ_7 and χ_{14} in the fundamental domain of G_2 at $\lambda_7 = 0$ and $\lambda_{14} = 0.1446$.

FIG. 10: (Colour online) Magnetisations $\langle\chi_7\rangle$ (upper curve) and $\langle\chi_{14}\rangle$ (lower curve) for various λ_7 at $\lambda_{14} = 0.13$.

$\lambda_{14,c} = 0$, $\lambda_{7,c} \approx -0.0975(75)$ of the fundamental model. Thus we have plotted the magnetisation in the vicinity of this first order transition from the ferromagnetic to the symmetric phase in Fig. 8. Note that even in the "symmetric" phase we find a non-zero magnetisation $\langle\chi_7\rangle$ which jumps at the critical coupling $\lambda_{7,c}$. This parallels the jump of the Polyakov loop in G_2 gluodynamics, see Fig. 1.

The phase diagram in Fig. 7 contains lines of second and first order transitions and 3 triple points. The full lines belong to first order and the dotted lines to second order transitions. Note that we may pass from the symmetric to the ferromagnetic phase via a first or via a second order transition. The transitions from the ferromagnetic to the anti-ferromagnetic phases AF1 and AF2 and between the anti-ferromagnetic phases are always of second order. In order to determine the orders of the transitions we calculated more than 30 histograms for the Polyakov loop distribution near the various phase transition curves and the changes of various 'order parameters' when one crosses the transition lines. A typical scatter plot is depicted in Fig. 9. It shows the distribution of χ_7 at a transition from the symmetric to the anti-ferromagnetic phase AF1 with critical couplings $\lambda_{7,c} = 0$ and $\lambda_{14,c} = 0.1446$. Without further analysis it is already clear that we are dealing with a first order phase transition.

The following Fig. 10 shows the behaviour of the magnetisations $\langle\chi_7\rangle$ and $\langle\chi_{14}\rangle$ near the transition from the symmetric to the ferromagnetic phase, which happens for $\lambda_{14} = 0.13$ and λ_7 between -0.18 and -0.12. Both expectation values vary continuously during the transition and this already suggests that the transition is of second order. This conclusion is further substantiated by the corresponding histograms for the distributions of χ_7 and χ_{14}.

V. THE G_2 POTTS MODEL

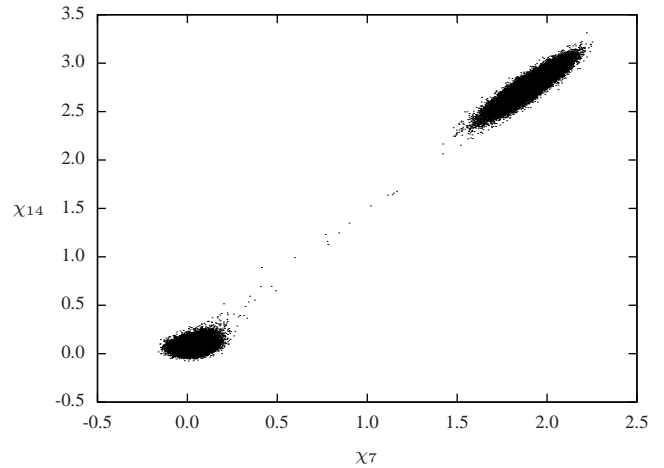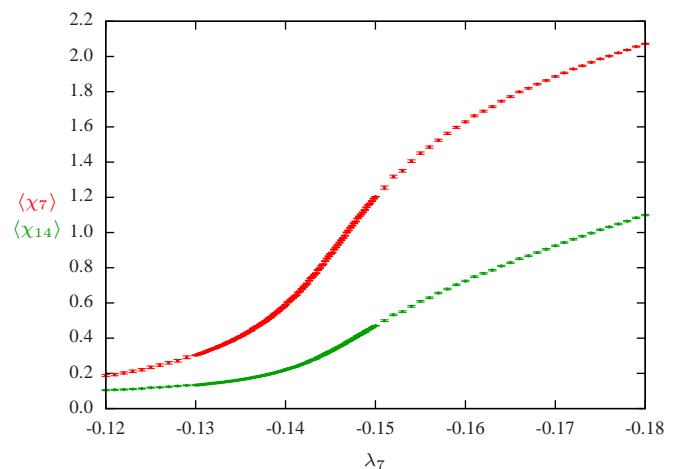After having collected sufficient information to reconstruct the full phase diagram of the fundamental continuous spin model with two effective couplings we now truncate the degrees of freedom further to arrive at a discrete spin model. In the case of the well-studied $SU(3)$ Polyakov loop models one projects a Polyakov loop $\mathcal{P}_{\boldsymbol{x}}$ onto the closest centre elements of $SU(3)$ and arrives at a $\mathbb{Z}_3$ Potts model with action (energy) given by

$$S_N = -\beta \sum_{\langle\boldsymbol{xy}\rangle} \delta(\sigma_{\boldsymbol{x}}, \sigma_{\boldsymbol{y}}), \quad \sigma_{\boldsymbol{x}} \in \mathbb{Z}_N. \qquad (33)$$

The continuous and discrete models have coinciding critical exponents at the second order anti-ferromagnetic phase transition and similar phase structures [18]. Motivated by these earlier successes we perform a similar reduction of the fundamental G_2 spin model and arrive at a discrete Potts-like G_2 spin model.

By projecting the values of $\mathcal{P}_{\boldsymbol{x}}$ to the three group elements with characters χ_7, χ_{14} lying at the extremal points of the fundamental domain in Fig. 2, we arrive at a model for the tree
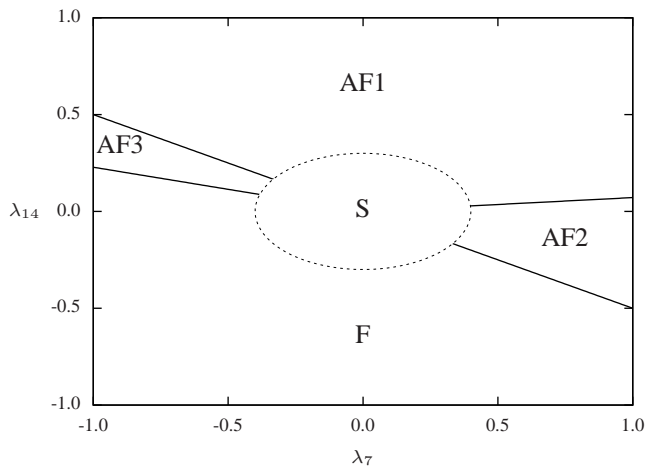
FIG. 11: The classical phase diagram of the discrete G_2 Potts model.

spins

$$\sigma_{\boldsymbol{x}} \in \left\{ \begin{pmatrix} 7 \\ 14 \end{pmatrix}, \begin{pmatrix} -1 \\ -2 \end{pmatrix}, \begin{pmatrix} -2 \\ 5 \end{pmatrix} \right\} \tag{34}$$

with nearest neighbour interaction determined by the Potts-type action

$$S_{\text{Potts}} = \sum_{\langle \boldsymbol{xy} \rangle} \sigma_{\boldsymbol{x}}^{\mathsf{T}} \begin{pmatrix} \lambda_7 & 0 \\ 0 & \lambda_{14} \end{pmatrix} \sigma_{\boldsymbol{y}} . \tag{35}$$

As expected, the classical phase diagram of the Potts-type model with discrete spins is similar to the diagram of the fundamental model with continuous spins. Depending on the sign of λ_7 and the slope $\xi = \lambda_{14}/\lambda_7$ we find the following phases and phase transition lines:

- For $\lambda_7 > 0$ and $\xi > -1/2$ and for $\lambda_7 < 0$ and $\xi > -47/206$ we find the *ferromagnetic phase* F with $\chi_{\text{e}}^{\mathsf{T}} = \chi_{\text{o}}^{\mathsf{T}} = (7, 14)$.

- For $\lambda_7 < 0$ and $-1/2 < \xi < -47/206$ we find the *anti-ferromagnetic phase* AF3 with $\chi_{\text{e}}^{\mathsf{T}} = (-1, -2)$ and $\chi_{\text{o}}^{\mathsf{T}} = (-2, 5)$.

- For $\lambda_7 > 0$ and $-1/2 < \xi < 1/14$ we find the *anti-ferromagnetic phase* AF2 wit $\chi_{\text{e}}^{\mathsf{T}} = (-2, 5)$ and $\chi_{\text{o}}^{\mathsf{T}} = (7, 14)$.

- For $\lambda_7 < 0$ and $\xi < -1/2$ and for $\lambda_7 > 0$ and $\xi > 1/14$ we find the *anti-ferromagnetic phase* AF1 with $\chi_{\text{e}}^{\mathsf{T}} = (-1, -2)$ and $\chi_{\text{o}}^{\mathsf{T}} = (7, 14)$.

The phase portrait is depicted in Fig. 11, where we have inserted by hand the expected symmetric phase for weak couplings. A striking difference between the diagrams in Fig. 3 and in Fig. 11 is the absence of the "transition phase" F → AF1 in the discrete model for which this phase does not exist by construction. Instead we find a third anti-ferromagnetic phase denoted by AF3 in Fig. 11. In addition, in the symmetric phase of the continuous spin model
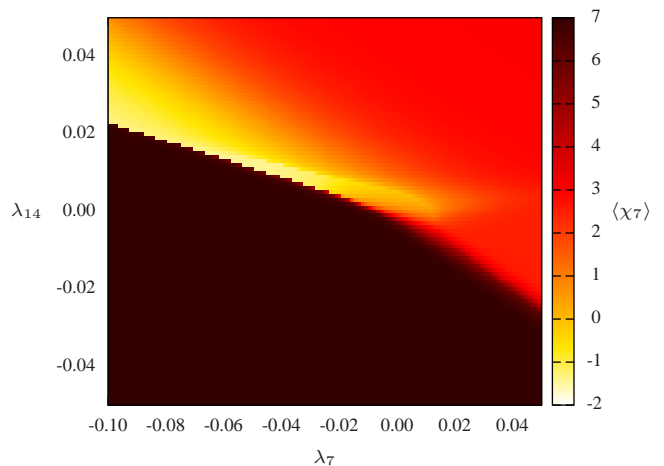

FIG. 12: (Colour online) Magnetisation $\langle \chi_7 \rangle$ of the discrete G_2 Potts model in mean field approximation.

$\langle \chi_7 \rangle \approx 0$ and in the symmetric phase of the discrete spin model $\langle \chi_7 \rangle \approx 4/3$.

Similarly as for the continuous model we calculated the phase diagram of the discrete model with the help of the modified mean field approximation. The contour plot for the magnetisation is depicted in Fig. 12. In the lower part of the plot we can see the ferromagnetic phase for which the Polyakov loops on both sublattices Λ_{e} and Λ_{o} are equal to the identity with very high probability.

The corresponding contour plot as obtained from Monte Carlo simulations is shown in Fig. 13. Again, the mean field approximation and the Monte Carlo simulations fully agree over the whole range of coupling constants. Note that the classical behaviour as depicted in Fig. 11 can be seen already for rather small coupling constants.
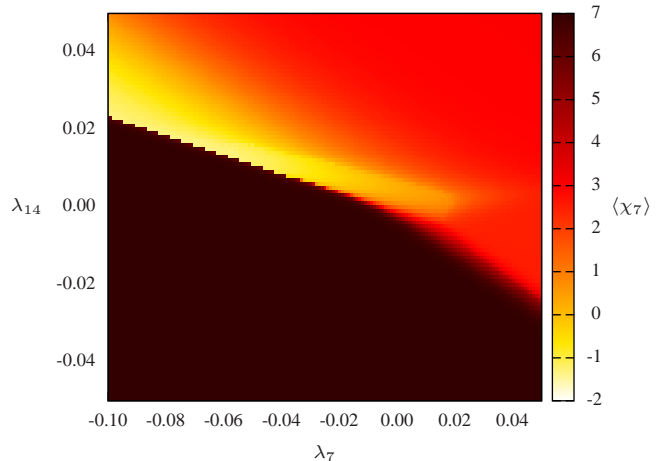

FIG. 13: (Colour online) Magnetisation $\langle \chi_7 \rangle$ of the discrete G_2 Potts model obtained via Monte Carlo simulation on an 8^3 lattice.

In order to localize the anti-ferromagnetic phases we also measured the staggered magnetisation introduced in (32). The resulting values on a grid in coupling constant space are plotted in Fig. 14. In accordance with the classical analysis we de-
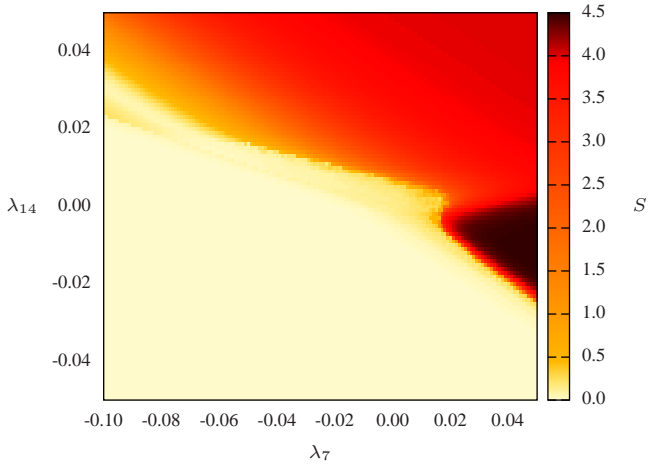
FIG. 14: (Colour online) Staggered magnetisation S of the discrete G_2 Potts model obtained via Monte Carlo simulation on an 8^3 lattice.

tect different anti-ferromagnetic phases for positive coupling constants in the upper right part of the phase portrait.

As concerning the relation between the Potts-type model and G_2 gluodynamics one caveat should be mentioned. In the discrete spin model there exists no real "symmetric phase" with a fixed expectation value of χ. Even for very weak coupling do the magnetisations $\langle\chi\rangle$ depend on the couplings. This is a remnant of the missing centre symmetry of G_2. Nevertheless, there exists a first order phase transition from one (would be symmetric) ferromagnetic phase at $\lambda_7 \approx \lambda_{14} \approx 0$ to a second ferromagnetic phase with $\mathcal{P}_x$ directed to the $\mathbb{1}$-element in G_2. Even in the simple discrete model we see very pronounced what happens in real G_2 gluodynamics. In the deconfining and confining phase there is a non-vanishing Polyakov loop, which still serves as *approximate* order parameter for confinement since it shows a steep jump at the transition point.

VI. CONCLUSIONS

Effective models for confinement with the Polyakov loop as macroscopic degree of freedom arise naturally from the strong coupling expansion of G_2 gluodynamics. Already the leading order continuous and discrete effective theories show a rich phase structure with two coexisting phases along transition lines and three coexisting phases at several triple points. The fundamental model with continuous spins and the Potts-type model with discrete spins share many properties, although in the absence of a centre symmetry they need not be in the same universality class. The continuous model exhibits a transition from the symmetric to the ferromagnetic phase with the same behaviour of the Polyakov loop as in G_2 gluodynamics, namely a steep jump from a small (but non-vanishing) Polyakov loop to a loop near the identity of G_2.

The classical, mean field and Monte Carlo analysis all lead to a coherent and consistent picture for both 3-dimensional effective theories. In particular, the prediction of the mean field approximation for $\langle\chi_7\rangle$ and $\langle|\chi_{7,\mathrm{e}} - \chi_{7,\mathrm{o}}|\rangle$ is in excellent agreement with the corresponding results obtained by detailed Monte Carlo simulations. This parallels our findings for $SU(3)$ in [18] and probably is due to the existence of tricritical points which lower the upper critical dimension in the vicinity of these points.

As concerning the relationship between the continuous effective models to the underlying G_2 gluodynamics we plan to apply inverse Monte Carlo techniques, preferably with demon methods, to determine the dependence of the coupling in the fundamental model on the gauge coupling. We hope to present the resulting curve $\lambda_7(\beta), \lambda_{14}(\beta)$ in a forthcoming publication. However we anticipate that for the critical Yang-Mills coupling β_c this curve will cross the transition line between the symmetric and ferromagnetic phases at small λ_{14} and negative $\lambda_7 \approx -0.1$ in Fig. 5.

[1] M. Pepe and U. J. Wiese, *Exceptional Deconfinement in G(2) Gauge Theory*, Nucl. Phys. **B768** (2007) 21 [arXiv:hep-lat/0610076].

[2] J. Greensite, K. Langfeld, S. Olejnik, H. Reinhardt and T. Tok, *Color screening, Casimir scaling, and domain structure in G(2) and SU(N) gauge theories*, Phys. Rev. **D75** (2007) 034501 [arXiv:hep-lat/0609050].

[3] L. Liptak and S. Olejnik, *Casimir scaling in G(2) lattice gauge theory*, Phys. Rev. **D78** (2008) 074501 [arXiv:0807.1390].

[4] J. Greensite, *The confinement problem in lattice gauge theory*, Prog. Part. Nucl. Phys. **51** (2003) 1 [arXiv:hep-lat/0301023].

[5] J. Danzer, C. Gattringer and A. Maas, *Chiral symmetry and spectral properties of the Dirac operator in G2 Yang-Mills Theory*, JHEP **01** (2009) 024 [arXiv:0810.3973].

[6] B. Svetitsky and L. G. Yaffe, *Critical Behavior at Finite Temperature Confinement Transitions*, Nucl. Phys. **B210** (1982) 423.

[7] L. G. Yaffe and B. Svetitsky, *First Order Phase Transition in the SU(3) Gauge Theory at Finite Temperature*, Phys. Rev. **D26** (1982) 963.

[8] C. Wozar, T. Kästner, A. Wipf and T. Heinzl, *Inverse Monte-Carlo determination of effective lattice models for SU(3) Yang-Mills theory at finite temperature*, Phys. Rev. **D76** (2007) 085004 [arXiv:0704.2570].

[9] L. Dittmann, T. Heinzl and A. Wipf, *An effective lattice theory*

for Polyakov loops, JHEP **06** (2004) 005 [`arXiv:hep-lat/0306032`].

[10] T. Heinzl, T. Kästner and A. Wipf, *Effective actions for the SU(2) confinement-deconfinement phase transition*, Phys. Rev. **D72** (2005) 065005 [`arXiv:hep-lat/0502013`].

[11] A. Velytsky, *Equilibrium criterion and effective spin models for finite temperature gauge theories*, Phys. Rev. **D78** (2008) 034505 [`arXiv:0805.4450`].

[12] C. Wozar, T. Kästner, B. H. Wellegehausen, A. Wipf and T. Heinzl, *Inverse Monte-Carlo and Demon Methods for Effective Polyakov Loop Models of SU(N)-YM*, PoS **LAT2008** (2008) 257 [`arXiv:0808.4046`].

[13] K. Holland, P. Minkowski, M. Pepe and U. J. Wiese, *Exceptional confinement in G(2) gauge theory*, Nucl. Phys. **B668** (2003) 207 [`arXiv:hep-lat/0302023`].

[14] A. J. Macfarlane, *The sphere S(6) viewed as a G(2)/SU(3) coset space*, Int. J. Mod. Phys. **A17** (2002) 2595.

[15] S. Uhlmann, R. Meinel and A. Wipf, *Ward identities for invariant group integrals*, J. Phys. **A40** (2007) 4367 [`arXiv:hep-th/0611170`].

[16] M. Creutz, *Microcanonical Monte Carlo Simulation*, Phys. Rev. Lett. **50** (1983) 1411.

[17] M. Hasenbusch, K. Pinn and C. Wieczerkowski, *Canonical demon Monte Carlo renormalization group*, Phys. Lett. **B338** (1994) 308 [`arXiv:hep-lat/9406019`].

[18] C. Wozar, T. Kästner, A. Wipf, T. Heinzl and B. Pozsgay, *Phase Structure of Z(3)-Polyakov-Loop Models*, Phys. Rev. **D74** (2006) 114501 [`arXiv:hep-lat/0605012`].